Proceedings of the 16th International Conference on Soil Mechanics and Geotechnical Engineering

doi:10.3233/978-1-61499-656-9-985

Image analysis of shallow foundation tests on sand ground and their FE-analysis using a new elasto-plastic model

Analyse d'image d'essai de fondations superficielles sur du sable et leur analyse par elements finis en utilisant un nouveau modèle elastico-plastique

S. Sreng, K. Ueno & A. Mochizuki
Department of Civil Engineering, Faculty of Engineering, Tokushima University, Japan
X. Ma
Department of Geotechnical Engineering, Faculty of Civil Engineering, Tongji University, China

ABSTRACT
In this study a series of loading tests on dense sand under a centrifugal force field was carried out, and a newly developed image analysis method with an accuracy of 0.2 pixels was used to observe detailed deformation of sand models. Loading tests were also analyzed using a two-dimensional FE-analysis with a developed double yield surface model, referred as the MMX-model. The calculated bearing capacity factor, N_γ, compares well with other reported data and that obtained from classical theory. Load-settlement relationships, displacement and strain distributions at pre-peak, peak, and post-peak stages obtained from the FE-analysis agree well with those obtained from the loading tests. The FE-analysis using MMX-model is concluded to be applicable to practical design work with sufficient accuracy to permit prediction of bearing capacity and deformation behavior of ground.

RÉSUMÉ
Dans cet article, une série de tests de charge sur des sols de sable dense par un champ de force centrifuge a été menée. Une nouvelle méthode d'analyse avec précision de 0.2 pixel a été développée et utilisée pour observer les détails des déformations des modèles de lits de sable. Ces tests ont également été soumis à une analyse par éléments finis à deux dimensions sur un nouveau modèle à double surfaces d' écoulement développé et référencé comme modèle MMX. Le coefficient de capacité portante calculé, N_γ, est conforme avec ceux obtenus par d'autres recherches et par la théorie classique. La relation entre charge et tassement, les distributions de déplacement et de déformation avant le pic, au pic, et après le pic, obtenus par l'analyse par éléments finis, est conforme avec les résultats des tests de charge. L'analyse par éléments finis utilisant le modèle MMX peut donc être utilisée dans des calculs pratiques avec une justesse suffisante pour prédire la capacité portante et le comportement de déformation du sol.

1 INTRODUCTION

This paper aims to present a combination of two subjects. The first is to show deformation mechanisms of sand ground under a footing in a centrifuge by using an image measuring method developed by the authors. The second is to demonstrate the accuracy of a numerical model with double yield surfaces, developed by the authors (Xiong et al. (2002)) and referred as the MMX-model, by comparing a series of analyzed results to those obtained by the centrifugal model tests.

With respect to visualization of the deformation of a model, this has been one of the fundamental challenges since the invention of the modern geotechnical centrifuge. Mikasa and Takada (1973) succeeded in visualizing deformation in sand by using a multi-exposure technique. Mikasa et al. (1977) established a photogrametoric target method and applied it to various deformation problems. The recent development of digital imaging technology has promoted application of image measuring in the geotechnical centrifuge, such as the 3-D target method by Taylor et al. (1998), CCIP method by Ueno et al. (2000), PIV by White et al. (2003) and the weight residual method by Michalowski and Shi (2003). In image measuring, coordination of measuring points and obtained displacement are discrete because of spatial restriction due to pixel size. This restriction results in serious error during the cumulative analyzing sequence. The authors developed a pixel-free method to overcome this disadvantage, and achieved an accuracy of 0.05 pixels for stationary error and 0.2 pixels for deformed image.

Bearing capacity problems are recognized as a bench mark to verify performance of FE-analysis. De Borst and Vermeer (1984) succeeded in calculating collapse loads and showed the possibility of FEM for limit analysis. Siddiquee et al. (1999) evaluated the performance of various types of constitutive models and concluded that models based on the double yielding concept gave the best fit for results of model loading tests. Xiong et al. (2002) succeeded in reproducing load-settlement curves by using the MMX model. In this paper, using the MMX model with an improved FEM program featuring stress correction and an iterative convergence procedure, the authors aim to demonstrate the load-settlement relationship and deformation and failure processes. The performance of the model and method developed is discussed.

2 EXPERIMENTAL STUDY

2.1 *Image analysis method*

An outline of the image analysis is as follows: displacement is computed between an original image and a deformed image. A small referential image with a size of $(2n+1)\times(2n+1)$ pixels is extracted from the original image at a region around an original coordinate (X_o, Y_o). Another small test image with the same size as the referential image is extracted from the deformed image around a tentative destination coordinate (X'_d, Y'_d). Coefficient of cross correlation R_{12} was computed from brightness of referential and test images v_{1i} and v_{2i} by using Eq. (1).

$$R_{12} = \frac{\sum_{i=1}^{(2n+1)^2} v_{1i} \cdot v_{2i}}{\sqrt{\sum_{i=1}^{(2n+1)^2} v_{1i}^2 \cdot \sum_{i=1}^{(2n+1)^2} v_{2i}^2}} \quad (1)$$

The tentative destination coordinate (X'_d, Y'_d) of the deformed image is changed to search for the point giving the maximum value of R_{12}. This point can be recognized as the destination coordinate (X_d, Y_d) corresponding to the original coordinate (X_o, Y_o) in the original image. Repeating the above procedure with a number of different original coordinates, whole combinations of (X_o, Y_o) and (X_d, Y_d) in an analyzed area can be obtained. A steepest gradient method was employed

to obtain precise results of 0.05 pixels for stationary error and 0.2 pixels for deformed images with strain smaller than 30%.

2.2 *Test material and Loading tests*

Material used in the tests was Toyoura sand. The characteristics are summarized as follows: Maximum grain size, 0.42 mm; mean grain size, 0.15 mm; maximum dry density, 1.655 g/cm^3; and minimum dry density, 1.363 g/cm^3. Sand models were constructed in a rectangular container with dimensions of 400×400×200 mm by an air pluviation method, and 1.6g/cm^3 of dry density (Dr=94%) was obtained.

Loading tests were conducted under a centrifugal force field of 20g using a model footing width B_0 measuring 20 mm. The centrifuge system used in this study was constructed at Tokushima University. It is of a balanced beam type with 1.55m of effective radius, developed by the authors. The model platform was designed to position the container perpendicular to the plane of rotation in order to reduce the influence of curvature of ground surface on acceleration direction. A digital camera with a resolution of 5.2 Mega pixels was set up in front of the ground model to photograph ground deformation during a loading test.

Vertical load with a constant settlement rate of 1mm/min was applied on a footing by using a hydraulic jack. Photographs of the deformation process of the ground used for image analysis were taken at every 0.5 mm of footing settlement.

The stress condition in the model ground was stabilized by applying four cycles of lowering-raising the centrifugal acceleration prior to loading. After these cycles, the centrifuge acceleration was raised again from 1g to 20g and maintained for one minute before the loading operation was initiated.

Images used for image analysis measured 2560×1920 pixels=4.9 Mega pixels, with a resolution of 0.167 mm/pixel.

3 NUMERICAL METHOD

3.1 *Outline of constitutive model*

The constitutive model used in this study is a newly developed double yield surface model, referred as MMX model (Xiong et al. (2002)). In this model, total strain increment $d\varepsilon_{ij}$ consists of three different parts: elastic strain increment $d\varepsilon_{ij}^{e}$, plastic compression strain increment $d\varepsilon_{ij}^{pc}$ and plastic shear strain increment $d\varepsilon_{ij}^{ps}$.

To represent the behavior of elastic deformation, isotropic and homogenous elasticity was assumed and material parameters in Hooke's law, E_e and ν, were determined from results of cyclic isotropic compression tests. Stress dependency of Young's modulus is expressed by a power function as follow:

$$E_e = E_0 \cdot (\sigma_m^* / \sigma_a)^{EN}, \quad \sigma_m^* = \sigma_m + c/\tan\phi \tag{2}$$

where σ_m is mean principal stress; E_0 and EN, experimental constants; and σ_a, referential stress, equal to 98 kPa.

To represent the behavior of plastic compression, the associated flow rule is adopted. The hardening rule is presented by Eq.(3), where $f_c = 3\sigma_m^*$ is the yield function; κ_{c0}, initial yield value; and κ_{ch}, hardening function defined by Eq.(4). In Eq. (4), a and b are experimental constants, H_c^p is the hardening parameter assumed to be the plastic work W_c^p (Eq. (5)), which is determined from ε_v^p -σ_m relationships obtained from cyclic isotropic compression tests.

$$F_c = f_c - (\kappa_{c0} + \kappa_{ch}) = 0 \tag{3}$$

$$k_{ch} = (H_c^p / a)^{1/b} \tag{4}$$

$$H_c^p = W_c^p = \int \sigma_{ij} \cdot d\varepsilon_{ij}^{pc} \tag{5}$$

The behavior of plastic shear deformation was expressed by a nonlinear hyperbolic relationship between octahedral shear stress τ_{oct} and plastic octahedral shear strain γ_{oct}^p ($\gamma_{oct} - \gamma_{oct}^e$). Shear modulus G_{oct} is determined from $\tau_{oct} - \gamma_{oct}^p$ relations, and is expressed as follow:

$$G_{oct} = A_g \cdot (\sigma_m^* / \sigma_a)^{SN} \cdot (1 - \tau_{oct} \cdot R_f / \tau_{octf})^2 \tag{6}$$

where A_g is an initial tangent of $\tau_{oct} - \gamma_{oct}^p$ relations; SN, experimental constant; R_f, failure ratio; and τ_{octf} is octahedral shear stress at failure specified by Mohr-Coulomb criterion. Considering results of plane strain compression tests by Mochizuki et al. (1988), the value of σ_{2f} is determined by assuming a coefficient of b=0.25, defined as $b = (\sigma_{2f} - \sigma_{3f})/(\sigma_{1f} - \sigma_{3f})$.

3.2 *Finite element analysis and its verification*

A two-dimensional plane strain FE-analysis program was developed to calculate the bearing capacity of a strip footing. An eight-node quadrilateral isoparametric element with reduced two-point Gaussian integration was employed. Stress correction was conducted when shear stress exceeded the failure criterion, and the exceeded stress was applied again. The modified Newton-Raphson (MNR) algorithm was employed to obtain the converged solutions. A preliminary investigation revealed that, when the displacement increment is less than 10^{-7}, the solution is accurately converged. Average number of iterations of every calculation step in which the solution converged were found to be approximately 5,000 cycles.

In order to verify the validity of the developed numerical analysis program, the bearing capacity factor, N_γ, was analyzed. Internal friction angles ϕ of 20, 25, 30, 35, 40, 45 degrees were adopted. FE-mesh consisted of 144 elements and 481 nodes, and its dimensions were $7.5B_0$×$7.5B_0$.

Figure 1(a) shows the relationships between normalized bearing capacity and footing settlement obtained from FE-analysis. It is noticed that the collapse loads can be calculated successfully by FE-analysis.

Figure 1(b) shows the comparison between calculated bearing capacity factor and the results of other researchers. This figure shows that the results of FE-analysis agree well with the results of other researchers. It is concluded that the FEM is sufficiently accurate in calculation of the bearing capacity.

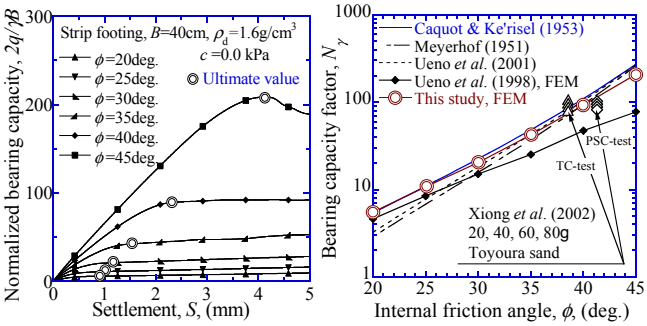

(a) Load-settlement relationships (b) Bearing capacity factor, N_γ

Figure 1. Verification of FE-analysis.

3.3 *FE-analysis of loading tests*

Figure 2 shows the FE-mesh (624 elements, 1973 nodes) and boundary conditions used in the analysis of loading tests.The mesh size was the same as that used in the image analysis.

Load was mobilized by applying prescribed vertical displacements to a footing with B_0=20 mm. The boundary condition under the footing was 'fixed' in a horizontal direction.

Material parameters used in the analysis of loading tests are listed in Table 1. Those for plastic shear were obtained from the σ_m-constant conventional triaxial compression test. Internal friction angle ϕ was increased two degrees and octahedral shear strain γ_{oct} was reduced to 50% in order to obtain those for plane-strain compression condition according to Mochizuki et al. (1988). All specimens used for these element tests were constructed by using an air-pluviation method.

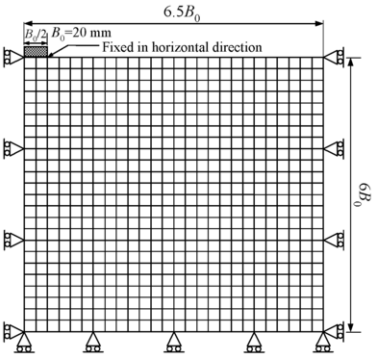

Table 1: Parameters

Elastic	E_0=238.0 MPa, EN=0.38, ν=0.35
Plastic compression	a=1.2× 10^{-4}, b=1.81, κ_{c0}=0.00
Plastic shear	A_g=91.8 MPa, SN=0.56, R_f=0.91, c=0.49kPa, ϕ=46.8°

Figure 2. FE-mesh and boundary conditions.

4 RESULTS AND DISCUSSIONS

Figure 3 compares relationships between normalized bearing capacity and footing settlement from FEM and those from loading tests under 20g of centrifugal acceleration. Settlement values at the peak of bearing capacity obtained by the FE-analysis coincide well with that of model tests, while the peak of bearing capacity by FE-analysis underestimates that indicated by model tests with a 20% scatter. The softening process shown in the test results is not simulated by the FE-analysis. However, some amount of decrease in load is observed in the load-settlement curve. This is attributed to redistribution of exceeded stress.

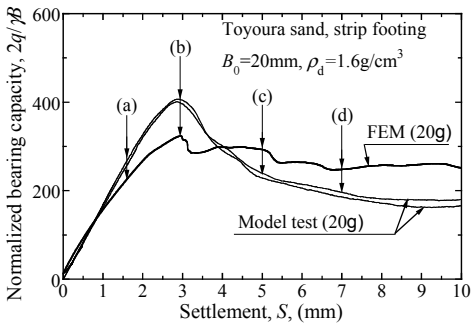

Figure 3. Relationships between normalized bearing capacity and footing settlement from FEM, compared with those from loading tests (20g).

Figure 4 shows a comparison between displacement distribution from loading tests and that from FE-analysis at point (a), (b), (c) and (d) in Fig. 3. In Fig. 4, the left-hand diagrams show an expansion process of contour lines of resultant displacement obtained from image analysis from model test. High deformation areas are shown by the bulbous shape of contour lines, before and at the peak concentration in the ground underneath the footing. Slip lines and zones in the ground are not observed before and at the peak. The movement in these stages is considered to be due to compaction behavior of ground under the footing due to settlement. The depth of the deformation area under the footing is equivalent to that of four times the depth of the footing width, B_0, and the width is four times that of B_0, which is the same conclusion presented by Xiong et al. (2001). After the peak, at the softening stage, the deformation expands horizontally, showing a prominent slip zone towards the right-hand side in the model tests.

In the FE-analysis, before and at the peak stage bulbous-shaped deformation areas under the footing arise, similar to those obtained from the model test. For stages after the peak, symmetrical movement horizontally was obtained from FE-analysis, while the prominent direction of movement is toward to the right-hand side in the model test.

Figure 5 shows a comparison between maximum shear strain distribution from loading tests and that from FE-analysis. Figures on the left-hand side show results observed in the model test. In stages before and at the peak, high shear zones, showing shear strains over 15%, are produced under both edges of the footing. It is clear that horizontal movements of solid blocks besides a wedge underneath the footing is developed predominantly after the peak. Areas with large shear strains expand in these stages, and are considered as a type of progressive failure.

In the FE-analysis shown in the right-hand diagrams, the expansion process of large shear strains is simulated correctly.

It is shown from the comparisons mentioned above, that the FE-analysis using the MMX-model can reproduce accurately the bearing capacity, the settlement at the peak, and the deformation process of a shallow foundation on a sand ground.

5 CONCLUDING REMARKS

From the good agreement achieved between experimental observation and both calculated deformation and load-settlement relationships, it is concluded that the proposed FE-analysis using MMX-model has sufficient accuracy and is valid for the prediction of bearing capacity and deformation behavior of ground in practical design.

ACKNOWLEDGEMENT

A part of this study was financially supported by Nishimatsu Construction Co., Ltd. The authors would like to express their thanks to Dr. Toshiyuki Hagiwara and Mr. Shinichiro Imamura of Nishimatsu Construction Co., Ltd. for their help. Contributions from Dr. Xiong Jie and Dr. Li Yuanhai are also acknowledged.

REFERENCES

De Borst, R. and Vermeer, P. A. 1984. Possibilities and limitations of finite elements for limits analysis, *Géotechnique*, 34, No. 2, 199-210.

Michalowski, R. L. and Shi, L. 2003. Deformation patterns of reinforced foundation sand at failure, *J. Geotech. Engrg.*, *ASCE*, Vol. 129, No. 6, 439-449.

Mikasa, M., Mochizuki, A. and Sumino, Y. 1977. A study on stability of clay slopes by centrifuge, *Proc. of The 9th ICSMFE*, Vol.2, 121-124.

Mikasa, M. and Takada, N. 1973. Significance of Centrifugal Model Test in Soil Mechanics, *Proc. of the eighth ICSMFE*, 273-278.

Mochizuki, A., Mikasa, M. and Takahashi, S. 1988. A New Independent Principle Stress Control Apparatus, *Advanced Triaxial Testing of Soil and Rock*, ASTM STP 977, 844-858.

Siddiquee, M. S. A., Tanaka, T., Tatsuoka, F., Tani, K. and Morimoto, T. 1999. Numerical Simulation of Bearing Capacity Characteristics of Strip Footing on Sand, *S & F*, Vol. 39, No. 4, 93-109.

Taylor, R.N., Robson, S. and Kuwano, J. 1998. An image analysis system for determining plane and 3-D displacements in soil models, *Proc. of the Int. Conf. Centrifuge 98*, 73- 78.

Ueno, K., Miura, K., Kusakabe, O. and Nishimura, M. 2001. Reappraisal of Size Effect of Bearing Capacity from Plastic Solution, *J. of Geotech. Geoenvir. Engrg.*, ASCE, 275-281.

Ueno, K., Takashima, S., Mochizuki, A. and Ma, X. 2000. Simple Measurement of Displacement Filed of Sand by Image Processing, *J. of JSCE*, No.666/III-53, 339-344. (in Japanese)

White, D. J., Take, W. A. and Bolton, M. D. 2003. Soil Deformation Measurement Using Particle Image Velocimetry (PIV) and Photogrammetry, *Géotechnique*, 53, No. 7, 619-631.
Xiong, J., Mochizuki, A., Ma, X. and Haratsuka, M. 2002. A New Double Loading Model and Analysis of Bearing Capacity on Sand, *J. of JSCE*, No.708/III-59, 107-116. (in Japanese)
Xiong, J., Mochizuki, A., Ma, X. and Tamaki, A. 2001. Bearing capacity tests of shallow foundation and deformation in sand, *The 46th Sympo. on Geotech. Engrg.* ,JGS, 253-258. (in Japanese)

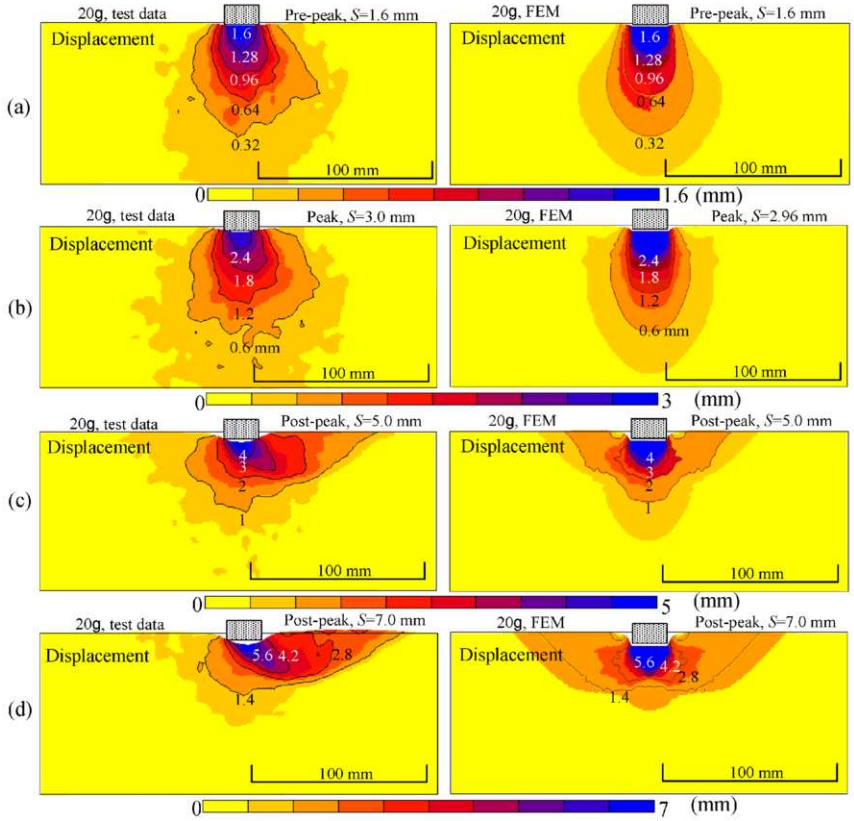

Figure 4. Measured and calculated displacement distribution for a 20g loading test on a dense Toyoura sand.

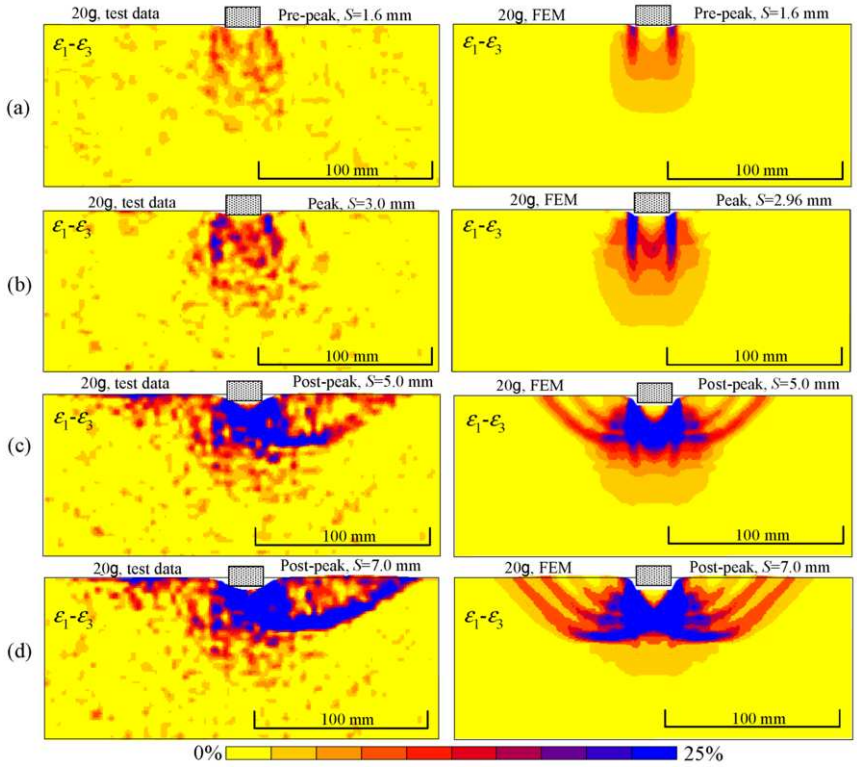

Figure 5. Measured and calculated maximum shear strain distribution for a 20g loading test on a dense Toyoura sand.